Arabian Journal of Geosciences (2021) 14:2052
https://doi.org/10.1007/s12517-021-08415-2

2ND CAJG 2019

Mapping and assessment of evapotranspiration over an oasis in arid ecosystem using remote sensing and biophysical modelling

Khalid Turk [1,2] · Faisal Zeineldin [1] · Abdullah S. Aljughaiman [1,3]

Received: 16 May 2020 / Accepted: 9 September 2021

Abstract

Evapotranspiration (ET) is an essential process for defining the mass and energy relationship between soil, crop and atmosphere. This study was conducted in Al-Ahsa Oasis, Eastern Region of Saudi Arabia, to estimate the actual daily, monthly and annual evapotranspiration (ETa) for different land-use systems using Landsat-8 satellite data during the year 2017/2018. Initially, six land-use and land-cover(LULC) types were identified: date palm, cropland, bare land, urban land, aquatic vegetation, and open water bodies. The Surface Energy Balance Algorithm for Land (SEBAL) supported by climate data was used to compute the ETa. The SEBAL model outputs were validated using the FAO Penman-Monteith(FAO P-M) method coupled with field observation. The results showed that the annual ETa values varied between 800 and 1400 mm year^{-1} for date palm, 2000 mm year^{-1} for open water and 800 mm year^{-1} for croplands. The validation measure showed a significant agreement level between the SEBAL model and the FAO P-M method with RMSE of 0.84, 0.98 and 1.38 mm day^{-1} for date palm, open water and cropland, respectively. The study concludes that the ETa produced from the satellite data and the SEBAL model is useful for water resource management at the oasis scale under the arid ecosystem.

Keywords Actual evapotranspiration (ETa) · Landsat-8 data · SEBAL model · Land-use and land-cover (LULC) · Arid ecosystem

Introduction

Evapotranspiration (ET) is an essential process for defining the mass and energy relationship between soil, crop and atmosphere (Allen et al. 2007). ET measurement is necessary for water management in arid ecosystems, and it has significant impacts on irrigation water requirement (Bastiaanssen et al. 2000; Anderson et al. 2012; Sun et al. 2019). ET is one of the most valuable variables to determine water balance in vast regions and affects future climate and land-use change (Rahimi et al. 2015; Qin et al. 2018). The ET can be estimated using many methods and techniques such as lysimeters, sap flow, eddy covariance, Bowen ratio and scintillometer, which were accurate and efficient at the field scale (Allen et al. 2011). However, these techniques cannot be used for large regional scale ET mapping due to prohibitive cost and logistical limitations (Singh and Senay 2016). Consequentially, remote sensing and biophysical modelling are adequate techniques for evaluating the ET patterns over large scale regions. The energy balance models used to estimate ET for semiarid areas combined with Landsat-8 images (Sun et al. 2019). The SEBAL model also applied to determine the distribution of the ETa for analysing water use patterns over a large basin in Kenya (Mutiga et al. 2010). However, the application of SEBAL in the Mara Basin of East Africa indicates that the ETa is measurable over different land-use types in data-scarce regions (Alemayehu et al. 2017). Daily ET monitoring using the SEBAL model also found to be possible for improving water resources decision support over an oasis in the desert ecosystem (Ochege et al. 2019).

Remote sensing and biophysical modelling were used in recent studies to estimate the ET in different Saudi

This paper was selected from the 2nd Conference of the Arabian Journal of Geosciences (CAJG), Tunisia 2019

Responsible Editor: Broder J. Merkel

✉ Khalid Turk
Khalidturk76@yahoo.co.uk; kturk@kfu.edu.sa

[1] Water Studies Center, King Faisal University, P. O. Box 400, Al-Ahsa 31982, Saudi Arabia

[2] Faculty of Agricultural and Environmental Science, University of Gadarif, P. O. Box 449, Gadarif, Sudan

[3] Department of Environmental and Natural Resources, College of Agricultural and Food Sciences, King Faisal University, P. O. Box 420, Al-Ahsa 31982, Saudi Arabia

Published online: 23 September 2021

Arabia regions. Mahmoud and Alazba (2016) estimated the ETa in the western and southern regions of Saudi Arabia during 1992–2014 using the SEBAL model, MODIS data and field observations. Also, in the eastern province of Saudi Arabia, the ET flux was evaluated over the alfalfa field using the METRIC and Landsat-8 data (Madugundu et al. 2017). Furthermore, in Saudi Arabia, remote sensing data used in combination with the surface energy balance system to estimate the daily ET rate and relative evaporation ratio of the irrigated agriculture in the Wadi ad-Dawasir area (Elhag and Bahrawi 2017).

The interactions of ET, climate change and land use are critical factors in soil water balance estimation and water resource management (Yang et al. 2021; Li et al. 2021). Precipitation and temperature estimations over different land-use systems can facilitate ET measurement in complex topography regions (Abdelmoneim et al. 2020; Almazroui et al. 2020). However, hydro-climatic parameters such as streamflow and rainfall might help determine the seasonal ET and water balance of a particular region (Abungba et al. 2020). The spatio-temporal analysis of climatic variables was important for quantifying the ET and management planning of water resources and sustainable agriculture (Gupta et al. 2021).

The Kingdom of Saudi Arabia (KSA) suffers a continuing water scarcity, and almost around 90% of the water budget used in the agricultural sector (ElNesr et al. 2010). Groundwater is the primary source of water in the KSA, considering the limited precipitation and high agricultural areas' demands. Moreover, the increased population of Saudi Arabia resulted in a significant increase in water use (Chowdhury and Al-Zahrani2015). Also, the diversity of the LULC in the arid region is critical to water consumption. Accordingly, for effective water resources management in these regions, the impacts of LULC on hydrology need to be assessed. Hence, precise information of the ETa is crucial for policymakers and water planners to develop and formulate strategies for agricultural water utilisation. Therefore, this study's objective is to assess the potential of Landsat-8 data and SEBAL model for estimating the daily, monthly and annual ETa under different LULC systems in Al-Ahsa Oasis of Saudi Arabia.

Material and methods

Study area

Al-Ahsa Oasis is located in the eastern part of Saudi Arabia and covers about 20,000 ha (Fig. 1). It is considered as one of

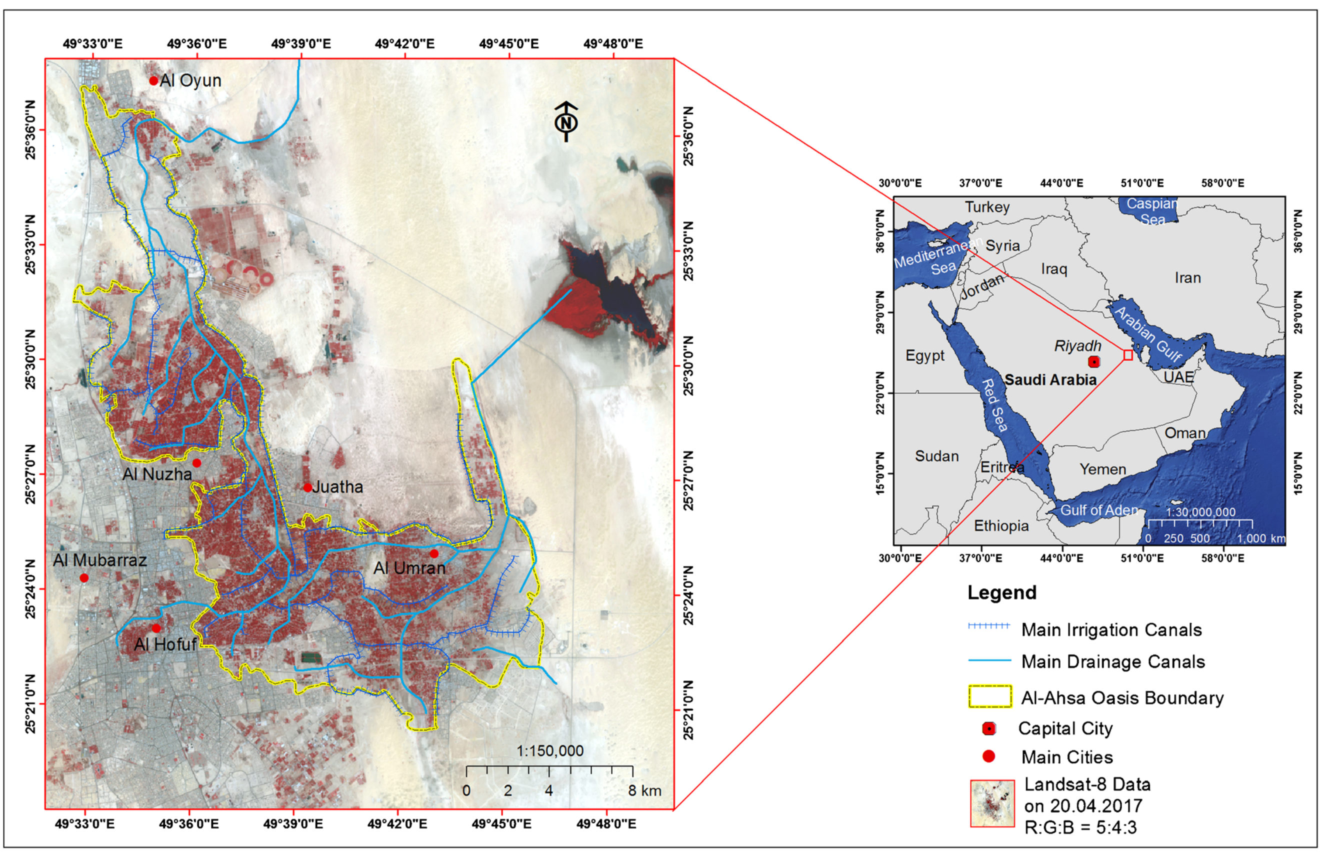

Fig. 1 Location of the study area

the largest and most important agricultural centres in Saudi Arabia, with an altitude range between 130 and 160 m above sea level (Allbed et al. 2018). The area's climate is arid, with air temperature exceeding 45 °C during the summer and reaching 5 °C in winter (Al-Taher 1992). The rainfall occurs mainly during winter, with an annual amount of less than 250 mm. The soil in the study area is dominated by sandy and sandy loam soils. Groundwater is the primary water source in the oasis and used mainly for irrigation, domestic and industrial purposes (Allbed et al. 2014). The land-use system in the study area is predominated by date palm plantation as the main agricultural activity. Also, the cropping of rice and vegetables is practised in the area.

Data

The data used in this study include remote sensing, climate information and field observations. They collected during April 2017–March 2018 to cover the summer and the winter season of the study area. The summer season is considered for April–September, while the winter is for October–March.

The Landsat-8 satellite imagery was obtained from the United States Geological Survey (USGS) website (https://earthexplorer.usgs.gov/). A total number of 22 images (path/row is 164/042) acquired to cover the entire study area, and the main characteristics of these data are shown in (Table 1). The obtained Landsat-8 images have a cloud cover of less than 10%, and they have been geometrically and radiometrically corrected. All images bands were resampled into a pixel size of 30 × 30m using the nearest neighbour method. A global digital elevation model (DEM) is generated from the Advanced Spaceborne Thermal Emission and Reflection Radiometer (ASTER) known as ASTER GDEM obtained from the USGS website. It is a 30-m-grid size DEM produced by the National Aeronautics and Space Administration (NASA) and the Ministry of Economy, Trade, and Industry of Japan (METI).

The collection of the climate data was from two meteorological stations located within the study area. These data include air temperature, relative humidity, wind speed, net radiation, precipitation and vapour pressure, and all data collections were on an hourly and daily basis.

The field observations include the identification of the main land-use system in the study area. Besides field notes, site descriptions and terrestrial photographs were taken to relate the site location to scene features.

LULC analysis

The LULC of the study area was classified based on the differences in the surface cover reflective behaviour of the different types. Accordingly, field surveys throughout the study area performed during the study period. A global positioning system (GPS) instrument was used to obtain accurate location point data for each LULC class included in the classification process. Consequently, the creation of training sites and generation of the spectral signature for the different LULC types were developed using the normalised difference vegetation index (NDVI) derived from Landsat-8 data (Mohajane et al. 2019). A total of 115 training sites were selected during the field survey. The supervised maximum likelihood classification (MLC) method was independently employed for the individual images. MLC was used widely in remote sensing for images classification (Mallick et al. 2014; Rahman et al. 2017; Oon et al. 2019). The accuracy assessment of the classified images was conducted using the ground control points (GCPs) collected during the field survey with a hand-held GPS. The GCPs were collected within 1 week of the image acquisition. Consequently, from the total collected 115 GCPs, 30% were used to validate the classified images. Also, visual

Table 1 Characteristics of Landsat-8 data used in this study (USGS 2019)

Sensor	Band type	Wavelength (μm)	Spatial resolution (m)
Operational Land Imager (OLI) and Thermal Infrared Sensor (TIRS)	Band 1, coastal aerosol	0.43–0.45	30
	Band 2, blue	0.45–0.51	30
	Band 3, green	0.53–0.59	30
	Band 4, red	0.64–0.67	30
	Band 5, near-infrared (NIR)	0.85–0.88	30
	Band 6, short-wave infrared 1 (SWIR-1)	1.57–1.65	30
	Band 6, short-wave infrared 2 (SWIR-2)	2.11–2.29	30
	Band 8, panchromatic	0.50–0.68	15
	Band 9, cirrus	1.36–1.38	30
	Band 10, thermal infrared 1 (TIRS-1)	10.60–11.19	100
	Band 10, thermal infrared 2 (TIRS-2)	11.50–12.51	100

interpretation of the unclassified satellite images supported with the field observations was used to validate the LULC maps. However, to reduce bias, the stratified random sampling method was adopted for the classified images (Mundia and Aniya 2006). Finally, the overall accuracy, user's and producer's accuracies and the Kappa statistic were derived from the error matrices (Congalton and Green 2009).

SEBAL model

The SEBAL model developed by Bastiaanssen et al. (1998) was used to calculate the actual evapotranspiration from Landsat-8 satellite images. The model key input data consist of satellite measurements of surface albedo, leaf area index (LAI), NDVI and surface temperature (Ts). Also, the DEM and land-use map were used as additional input data. The DEM was applied for topographic and atmospheric correction (Malbéteau et al. 2017). However, the land-use map was used mainly to differentiate between LULC types that exist in the study area. SEBAL model provides accurate estimations of ET for relatively flat agricultural areas. However, where there are significant reliefs and a wide range of slopes and aspects, the SEBAL mountain model was developed to correct the slope, aspect and elevation in the ET's computations process (Allen et al. 2012). Therefore, the DEM was required to provide elevation data. In addition to the satellite data, the SEBAL model requires minimum inputs of routine weather data (see the Data section). Figure 2 shows a flowchart that describes the SEBAL model process. The SEBAL model scripts were formed using the Spatial Modeler Tool of the ERDAS IMAGINE 9.2 software, and the ArcGIS 10.2 software was used for data mapping and visualisation.

The SEBAL algorithm computes the latent heat flux as the residue of the energy balance equation (Bastiaanssen et al. 1998; Bastiaanssen et al., 2005; Allen et al. 2013):

$$\lambda ET = \mathrm{R_n} - \mathrm{G} - \mathrm{H} \tag{1}$$

where R_n is the net radiation over the surface (W/m^2), G is the soil heat flux (W/m^2), H is the sensible heat flux (W/m^2), λET is the latent heat flux (W/m^2) and λ is the latent heat of vaporisation (J/Kg).

The net radiation (R_n) was calculated using surface reflectance and surface temperature (T_s) derived from satellite imagery. The R_n computed as follows:

$$\mathrm{R_n} = \mathrm{R_s}\downarrow - \propto \mathrm{R_s}\downarrow + \mathrm{R_L}\downarrow - \mathrm{R_L}\uparrow - (1-\varepsilon_0)\,\mathrm{R_L}\downarrow \tag{2}$$

where $R_s\downarrow$ is the incoming short wave radiation (W/m^2) (solar radiation), $\propto$ is the surface albedo (dimensionless), $R_L\downarrow$ is the incoming longwave radiation (W/m^2), $RL\uparrow$ is the outgoing longwave radiation (W/m^2) and ε_0 is the surface thermal emissivity (dimensionless). The calculation of these radiations was performed in Eqs. 3–5(Allen et al. 2006):

$$RS\downarrow = G_{sc}.\cos\theta.r.\tau_{sw} \tag{3}$$

$$RL\uparrow = \varepsilon_0.\sigma.T_s^4 \tag{4}$$

$$RL\downarrow = \varepsilon_\propto.\sigma.T_\propto^4 \tag{5}$$

where G_{sc} is the solar constant (1367 W/m^2), and cosθ is the cosine of the solar incidence angle, r is the Earth-Sun distance

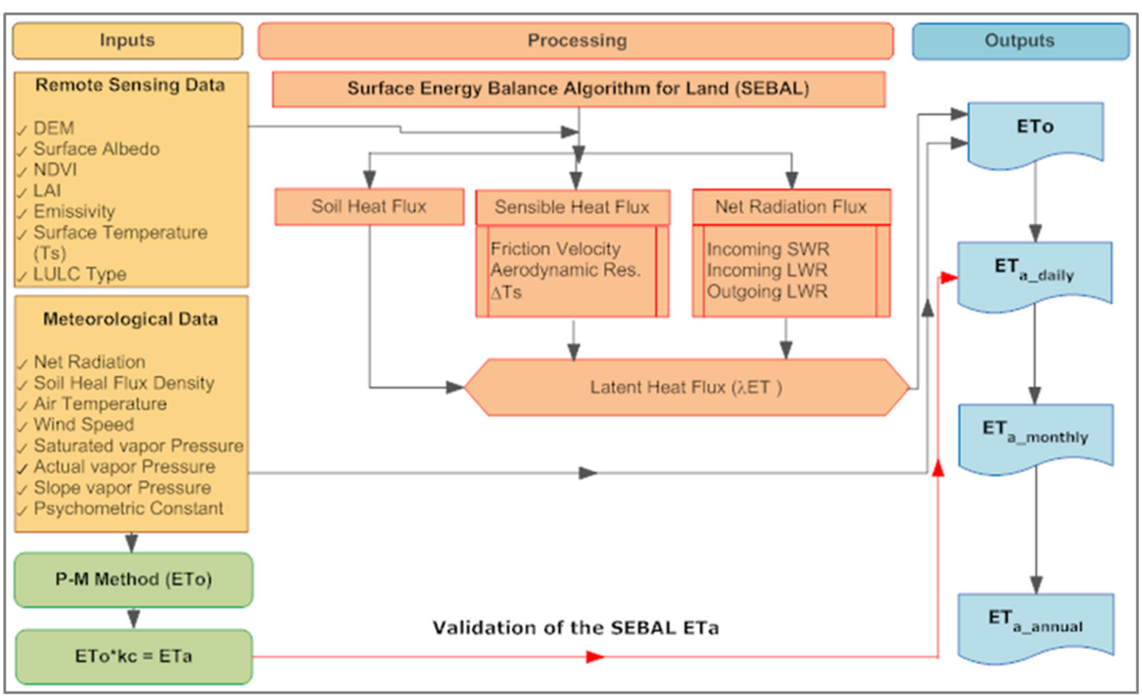

Fig. 2 A flowchart explains the SEBAL model process

(dimensionless), and τ_{sw} is atmospheric transmissivity. RSI↓ values range from 200 to 1000 W/m^2, depending on the image's time, location and local weather conditions (Allen et al. 2012). σ is the Stefan-Boltzmann constant (5.67×10^{-8} W m^{-2} K^{-4}), T_s is the surface temperature (K), ε_α is the atmospheric emissivity and $T_\propto$ is the atmospheric temperature (K). The empirical Eq. 6 was used for calculating the $\varepsilon_\propto$ (Allen, 2012).

$$\varepsilon_\propto = 0.85 \times (-ln\ \tau_{sw})^{0.09} \tag{6}$$

The soil heat flux (G) is the heat flux rate stored or released into the soil and vegetation due to conduction. The ratio G/R_n was computed using Eq. 7 developed by Bastiaanssen et al. (2000):

$$\mathrm{G/R_n} = \frac{T_s}{\propto}\left(0.0038 + 0.0074\propto^2\right)\left(1{-}0.98NDVI^4\right) \tag{7}$$

where T_s is the surface temperature (C°), ∝ is the surface albedo, and NDVI is the Normalised Difference Vegetation Index (ranged between −1 and +1). NDVI values between 0 and 0.2 correspond to bare soil or very sparse vegetation. The values greater than 0.2 represent vegetated areas. The typical estimates of G/R_n assumed to be 0.5 for water, 0.05–0.4 for agriculture and 0.2–0.4 for bare soil (Allen et al. 2012). The NDVI was calculated from Eq. 8(Mohajane et al. 2019):

$$NDVI = \frac{(NIR{-}RED)}{(NIR + RED)} \tag{8}$$

where NIR is the reflectance in the near-infrared band, which corresponds to band 5 in Landsat-8 data, while the RED reflectance corresponds to band 4.

The sensible heat flux (H) is the heat loss rate to the air by convection and conduction due to a temperature difference. H was determined using the aerodynamic-based heat transfer equation as follows (Bastiaanssen 2000):

$$H = \frac{\left(\rho \times \mathrm{C_p} \times dT\right)}{\mathrm{r_{ah}}} \tag{9}$$

where ρ is air density (kg/m^3), C_p is air specific heat (1004 J/kg/K), dT(K) is the temperature difference (T_1 and T_2) between two heights (Z_1 and Z_2) and r_{ah} is the aerodynamic resistance to heat transport (s/m). The r_{ah} is computed for neutral atmospheric stability conditions as follows:

$$\mathrm{r_{ah}} = \frac{ln\left[\frac{Z_2}{Z_1}\right]}{u* \times\ k} \tag{10}$$

where Z_1 and Z_2 are heights in metres above the zero-plane displacement of the vegetation, $u*$ is the friction velocity (m/s), which quantifies the air's turbulent velocity fluctuations. K is von Karman's constant (0.41). $u*$ is computed using the logarithmic wind law for neutral atmospheric conditions:

$$u* = \frac{ku_x}{ln\left[\frac{Z_x}{Z_{om}}\right]} \tag{11}$$

where u_x is the wind speed (m/s) at height Z_x, and Z_{om} is the momentum roughness length (m). The wind speed at the 200 m (blending height) is assumed not to affect the underlying surface roughness and is assumed to be constant over the entire image or sub-image.

The instantaneous value of ET in equivalent evaporation depth was computed as follows:

$$\mathrm{ET_{inst}} = 3600\ \frac{\lambda\mathrm{ET}}{\lambda} \tag{12}$$

where ET_{inst} is the instantaneous ET (mm/h), 3600 is the conversion from seconds to hours, λET is the latent heat flux (W/m) consumed by ET, ρw is the density of water (1000 kg/m^3) and λ is the latent heat of vaporisation (J/kg) and was computed as follows:

$$\lambda = \left[2.501{-}0.00236\ (\mathrm{T_s}{-}273.15) \times 10^6\right] \tag{13}$$

The reference ET fraction (ET_0F) or crop coefficient (kc) was calculated based on ET_{inst} for each pixel, and ET_0 was obtained from local ground weather stations.

$$\mathrm{ET_0\,F = ET_{inst}/ET_0} \tag{14}$$

The daily values of ET (ET_{24}) (mm/day) for each pixel was calculated as follows:

$$\mathrm{ET_a = ET_0\,F \times ET_0 24} \tag{15}$$

where ET_0F is the reference ET fraction, $ET_0 24$ is the cumulative alfalfa reference for the day (mm/day) and ET_a is the actual evapotranspiration for the entire 24-h period (mm/day).

The actual monthly and annual ET was calculated using daily ET data as follows (Allen et al. 2012):

$$\mathrm{ET_{a,period}} = \sum_{i=m}^{n} \mathrm{ET_0\,F \times ET_0 24} \tag{16}$$

$$\mathrm{ET_{a,annual}} = \sum ET_{a,\mathrm{period}} \tag{17}$$

Allen et al. (2007) showed that one cloud-free satellite image per month is sufficient to develop ET_0F curves for seasonal ET_a estimations.

Data analysis and model validation

The produced ETa from Landsat-8 images and SEBAL model was validated using the FAO P-M method (Allen et al. 1998). This method was used to calculate the reference crop evaporation (ET_0) from the actual climate data in the study area as follows:

$$ET_0 = \frac{0.408\Delta(Rn-G) + \gamma \frac{900}{T+273} U2(es-ea)}{\Delta + \gamma(1+0.34U2)} \tag{18}$$

where ET_0 is reference evapotranspiration (mm/day), Δ is slope vapour pressure curve (kPa/°C), γ is psychrometric constant (kPa/°C^{-1}), T is mean daily air temperature at 2-m height (°C), $U2$ is the wind speed at 2-m height (m/s), es is saturation vapour pressure (kPa), ea is actual vapour pressure (kPa) and ($es - ea$) represents the saturation vapour pressure deficit (kPa).

The crop coefficient (Kc) is for the different croplands and the open water determined based on Allen et al. (1998). The ET_0 obtained from the FAO P-M method and the kc were used to calculate the ET_a depending on actual weather data as follows:

$$ET_a = ET_0 \times kc \tag{19}$$

The ET_a resulted from the FAO P-M method was used to validate the ET_a obtained from the SEBAL model. Many studies validated the estimation of the SEBAL ET_a using the FAO P-M method, like cultivated land in Iran (Rahimi et al. 2015), a blown-sand region in China (Kong et al. 2019) and the Nile Delta in Egypt (Elnmer et al. 2019).

A linear correlation and the root mean square error (RMSE) between the measured (FAO P-M) and the SEBAL daily ET_a was computed (Bellvert et al. 2018). The RMSE was calculated as follows (Ghaderi et al. 2020):

$$RMSE = \sqrt{\frac{\sum_{i=1}^{N} (O_i - P_i)^2}{N}} \tag{20}$$

where O_i represents the observed values of the FAO P-M method as the standard model; P_i represents the estimated values from the SEBAL algorithm; and $\overline{O_i}$ and $\overline{P_i}$ are the mean values from the FAO P-M method and SEBAL model, respectively.

The seasonal validation accuracy of the mean daily ETa between the FAO P-M method and SEBAL model was made using the relative error (RE) approach. The RE was calculated using the equation adapted from Kong et al. (2019):

$$RE = \left| \frac{V_A - V_E}{V_E} \right| \times 100\% \tag{21}$$

where RE is an absolute value (%); V_A is the actual value observed (FAO P-M method); V_E is the predicted value (SEBAL model).

The Microsoft Excel 2010 software was used for statistical analysis and producing charts of the data (Baskauf 2016).

Results and discussion

LULC mapping

The study area's LULC map showed that the main identified classes were the date palm, cropland, bare land, urban land, aquatic vegetation and water (Fig. 3). The area occupied by each LULC type within the oasis boundaries is shown in Table 2. The date palm covers about 40% of Al-Ahsa Oasis since it is the most important land-use class for the local and national economy. Croplands used only 19% of the oasis area, and it is dominated by rice and vegetables. However, the bare land class occupies around 39% of the oasis area. Bare lands dominated by desert and rock outcrops also occurred in this class. Most of the urban land occurs on the oasis periphery, as most oasis land is under agricultural use. The aquatic vegetation and water classes occupy together an area of about 67 ha within the oasis boundary. However, these classes relatively cover large areas outside the oasis, mainly due to the accumulation of drain water from the oasis agricultural lands. Al-Dakheel(2011) reported that the total cultivated land in the oasis was 7000 ha, and about 92% of it covered with date palm. Furthermore, the time trend of NDVI over the study area indicated that most of the LULC types could be differentiated throughout the study period (Fig. 4). Combining the MLC method and the NDVI was successfully applied for mapping the LULC changes in Morocco (Mohajane et al. 2019).

The overall classification accuracy of the LULC map was 89%, with a kappa index of 87%, while the user's and producer's accuracies differed along with LULC types (Table 2). This accuracy level indicates that this study's classification method effectively produced a compatible LULC map over the study area.

The actual evapotranspiration

The spatial distribution of the daily ETa over Al-Ahsa Oasis from 20 April 2017 to 22 March 2018 is shown in Fig. 5. The temporal patterns of the daily ETa showed that the highest values were observed during the peak summertime in July and August. The mean daily ETa values for the different LULC types in the oasis are shown in Fig. 6. It is clear that the daily ETa for the water bodies and aquatic vegetation was between 5.6 and 8.7 mm day^{-1} in summer and about 2.3–5.6 mm day^{-1} in winter. However, the date palm and croplands showed daily ETa of 3.5–8.0 and 2.0–3.6 mm day^{-1} for the winter and summer, respectively.

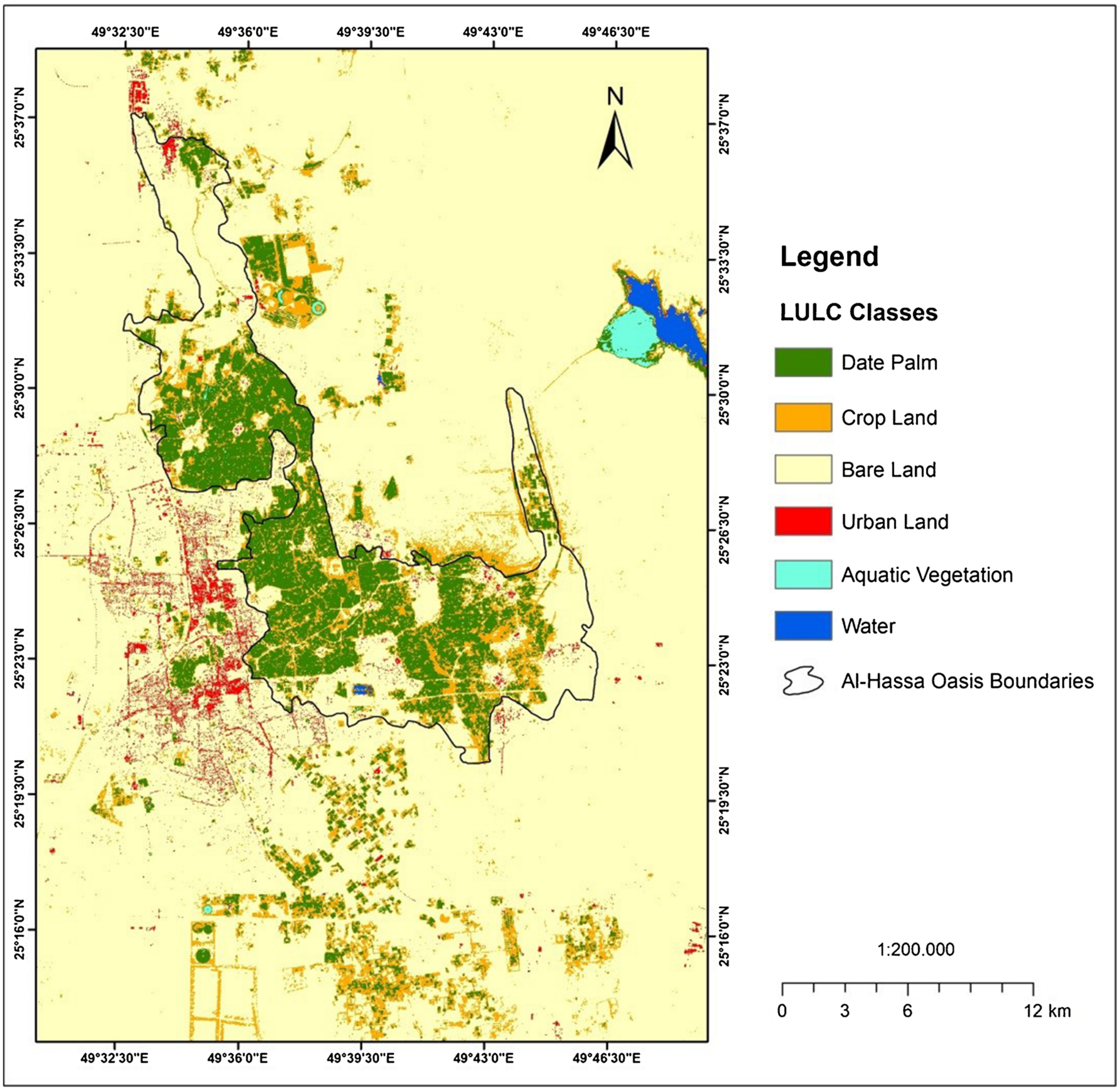

Fig. 3 LULC map of the study area

The variability of the daily ETa values for the date palm and cropland during the summer and winter times mainly attributed to the irrigation water distribution, soil salinity, drainage, and agricultural practices and their impact on moisture and salinity in the root zone. Under Saharan oasis conditions, soil texture, plot size and farmers' practices in particular

Table 2 Areas and accuracy assessment of LULC classes within Al-Ahsa Oasis boundary

LULC	Area		Classification accuracy (%)	
	Hectare	%	User's	Producer's
Date palm	8820	40.1	95	94
Cropland	4199	19.1	83	81
Bare land	8636	39.2	95	93
Urban land	278	1.3	82	86
Aquatic vegetation	37	0.2	75	92
Water	30	0.1	100	100
Overall			89	
Kappa Statistic			87	

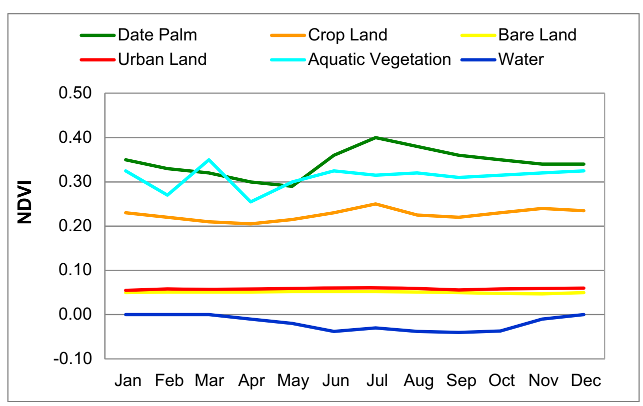

Fig. 4 NDVI time trend for the different LULC types

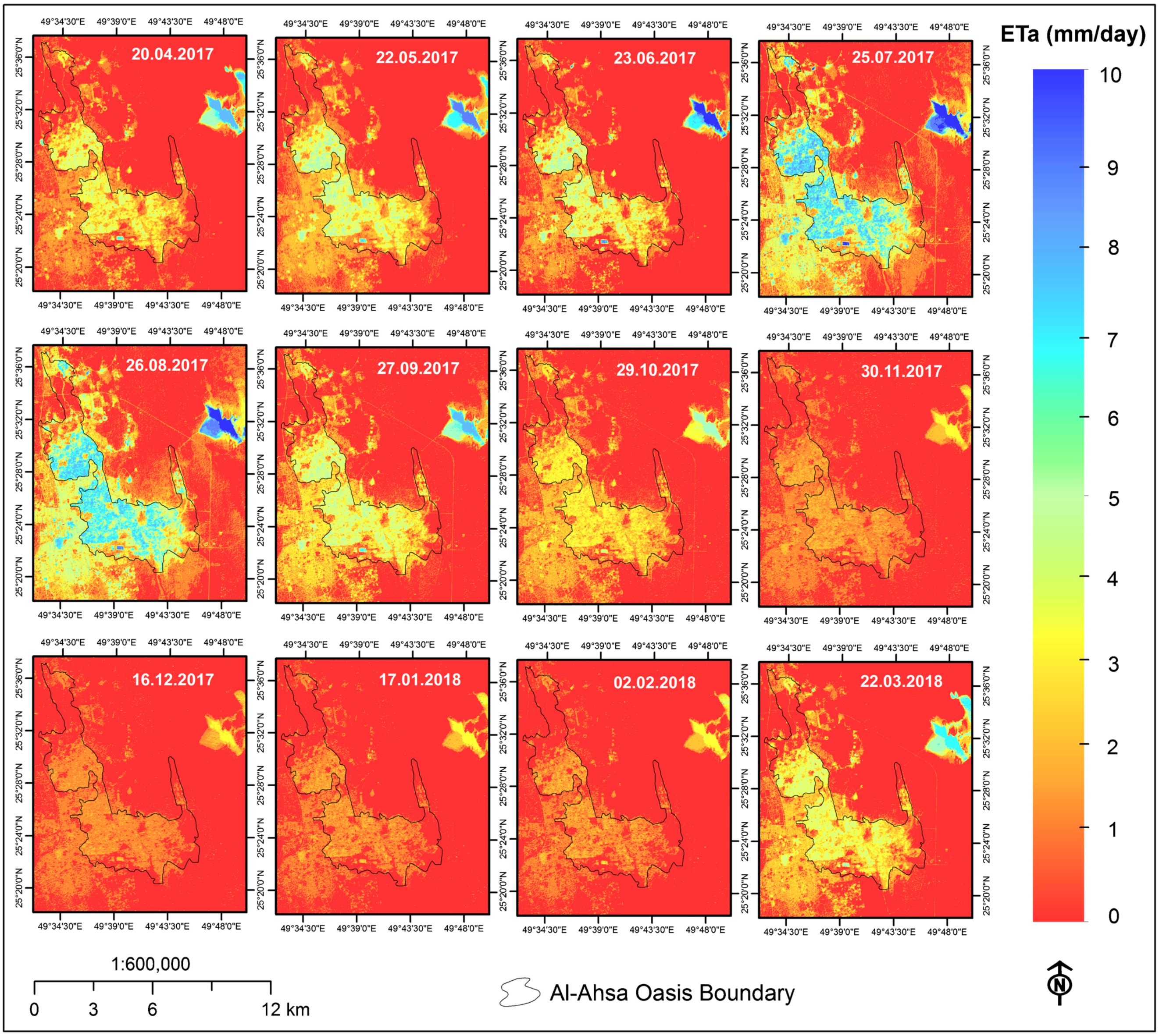

Fig. 5 The spatial distribution of the daily ETa over Al-Ahsa Oasis

irrigation found to have significant effects on the daily ETa (Haj-Amor et al. 2017). In Saudi Arabia, the daily ETa of date palm was observed to decrease during winter and increase during summer, depending on the crop's growth stage (Carr 2013). The daily water consumption of major cropping systems in Saudi Arabia varied spatially depending on cropping practices and climatic conditions (Mahmoud and Alazba 2016).

The mean daily ETa for the urban land ranged from 1.3 to 4.5 mm day^{-1} throughout the study period (Fig. 6). The urban land is covered with some lanes and parks that make seasonal variations of the daily ETa within the study area. Nevertheless, the low values of the daily ETa showed in the bare land mainly resulted from the sparse vegetation in this land-use system.

The variation of the daily ETa estimates for the different LULC types under the oasis-arid ecosystem indicates that they change significantly throughout the seasons (Ochege et al. 2019).

Figure 7 shows the spatial pattern of the monthly and annual ETa across Al-Ahsa Oasis. The high rates of the ETa found to be between 80 and 200 mm month^{-1} during July, August and September for the water, aquatic vegetation, date palm and cropland. However, at the beginning of the summer in April, May and June, the ETa rates were 60–100 mm month^{-1} for the same LULC types. Nevertheless, in the winter during Oct 2017–Mar 2018, the ETa ranged between 40 and 140 mm month^{-1} for the water, aquatic vegetation, date palm and cropland land-use systems.

Fig. 6 Temporal variation of mean daily ETa for different LULC systems in Al-Ahsa Oasis

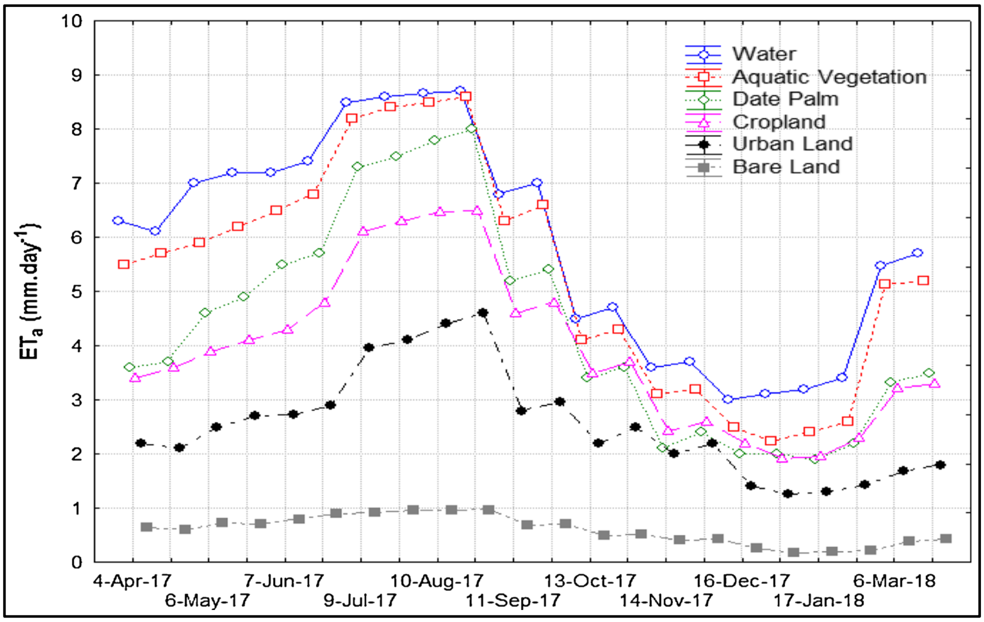

The mean annual ETa produced by the SEBAL model for the different LULC types in Al-Ahsa Oasis is shown in Fig. 8. The ETa rates of date palm trees ranged from 800 to 1400 mm year^{-1} during Apr. 2017 to Mar. 2018. The annual water consumption for date palm was highly variable. This might be attributed to the type of irrigation system and the age variations of date palm trees along the oasis.

The open water evaporation loss was around 2000 mm year^{-1}, while an average of 1600 mm year^{-1} was evaporated from aquatic vegetation. Nevertheless, croplands showed a lower annual ETa of 800 mm year^{-1} compared to the date palm. The main crops like rice and vegetables can be cultivated during a particular time of the year in the oasis; therefore, croplands

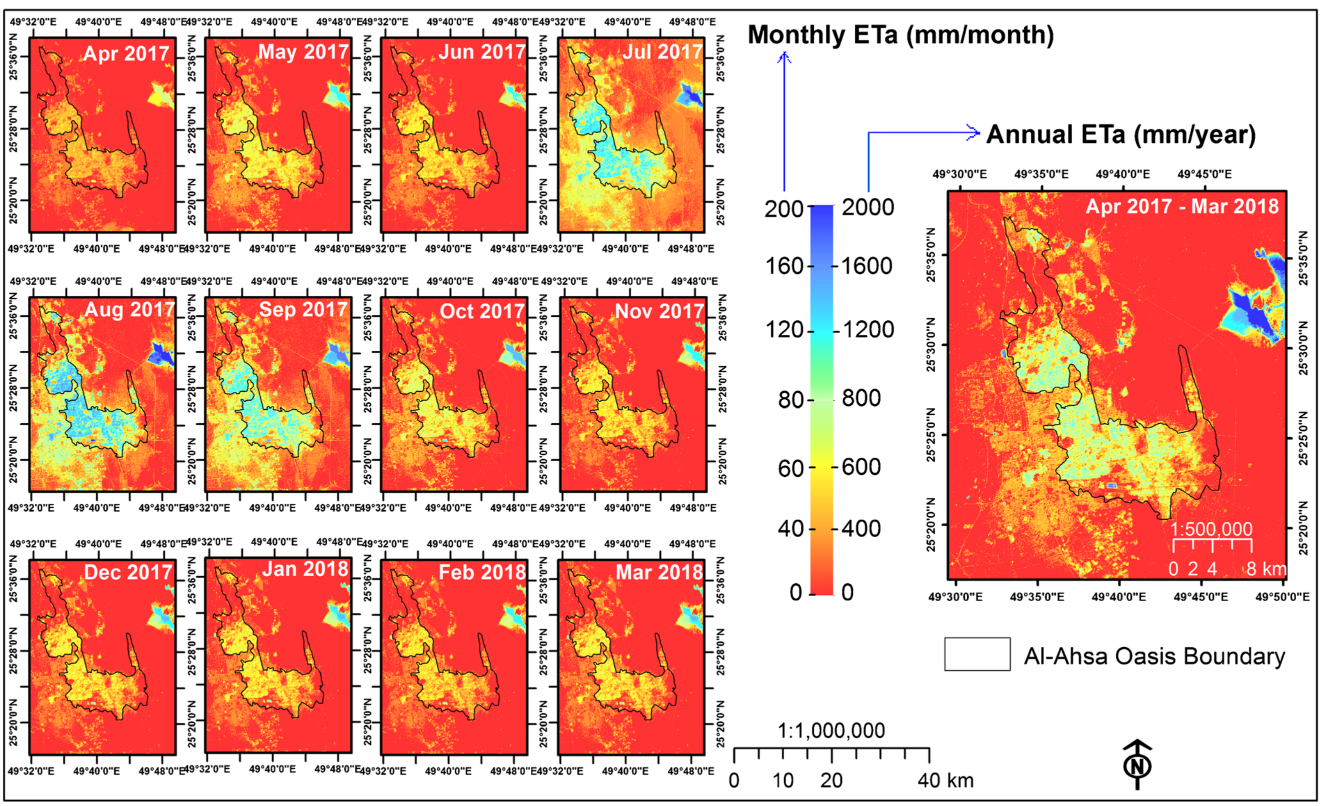

Fig. 7 The spatial patterns of the monthly and annual ETa along Al-Ahsa Oasis

Fig. 8 Mean annual ETa produced by SEBAL for the different LULC types in Al-Ahsa Oasis during April 2017–March 2018. Bars denoted standard error

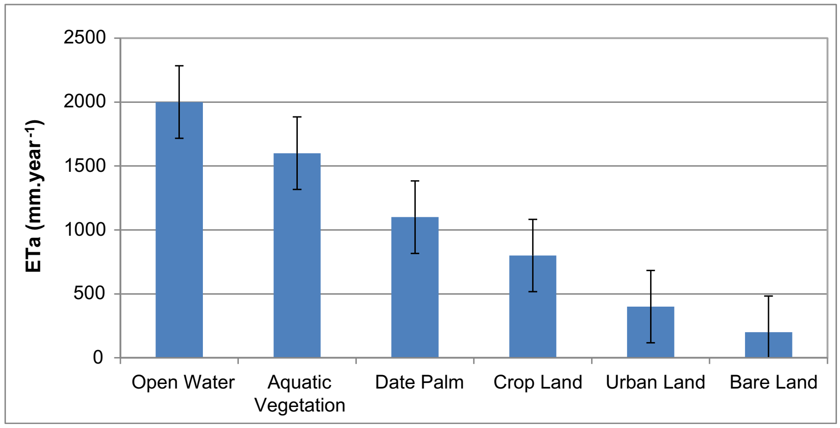

showed relatively low annual ETa compared to date palm areas.

The annual ETa of urban lands was 400 mm year^{-1}. Urban lands are affected by the irrigation of trees, lanes and parklands, which resulted in the consumption of a large amount of the oasis groundwater. The annual evaporation from bare lands was very low (200 mm year^{-1}) and less than the long-term average rainfall. Most of the bare lands in the study area are covered with dunes, and they characterised by low levels of vegetation coverage and low water contents on the soil surface (Kong et al. 2019). Also, very low rates of ETa from bare soil are observed in the western and southern parts of Saudi Arabia (Mahmoud and Alazba 2016).

Validation of SEBAL model

The FAO P-M was used as a standard method to validate the SEBAL model (Sentelhas et al. 2010; Kong et al. 2019). The validation measurement for ETa between the SEBAL model and FAO P-M method for the different land-use systems is shown in Fig. 9. A significantly high level of agreement can be observed between the two methods for the selected LULC types. The RMSE for the most validated LULC system in the study area found to be less than 1.0 mm day^{-1}. However, the RMSE was slightly higher for cropland areas (Fig. 9d), mainly due to the method used for calculating the crop coefficient (kc) for the different crop types within the croplands system.

Fig. 9 Linear correlation between the FAO P-M and SEBAL model for the different LULC types. **a** Open water. **b** Aquatic vegetation. **c** Date palm. **d** Cropland

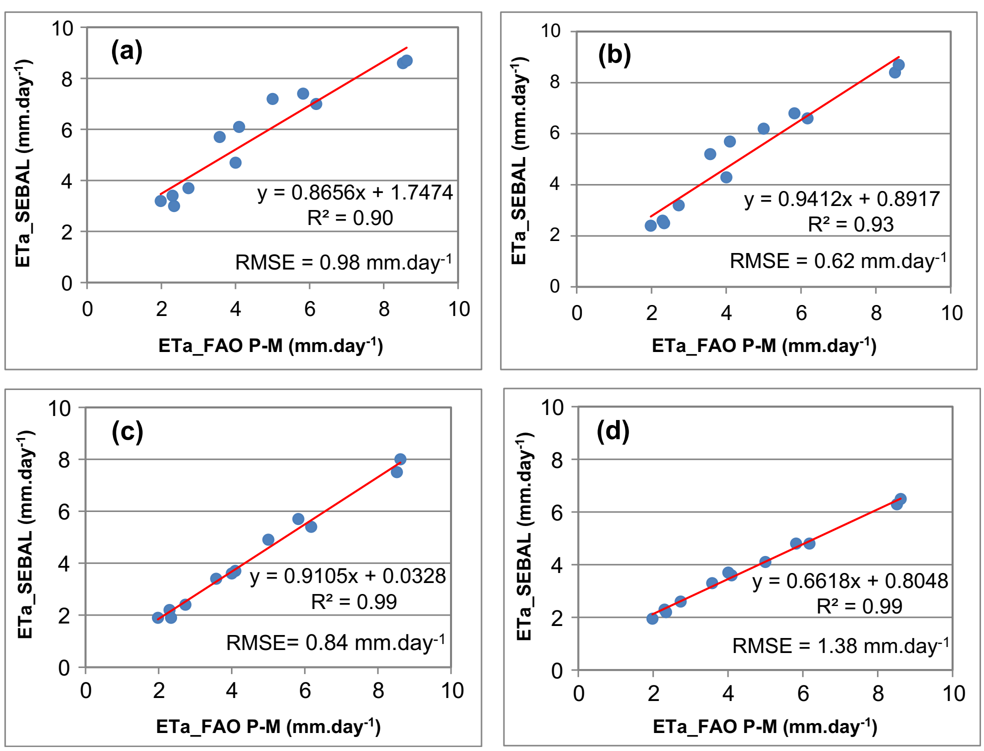

The SEBAL model does not require kc information because the model biophysical properties estimated Kc as part of the SEBAL process. However, the FAO P-M computed kc based on the characteristics and climatic regions for the different crops. Accordingly, the kc of vegetables (tomato and cucumber) ranged between 0.5 and 1.15, and for the rice, it was 1.0–1.35 (Allen et al. 1998). Nevertheless, the date palm's kc was in the range of 0.9–0.95, while it was 1.05 for the open water (Allen et al. 1998). Also, the kc of crops can vary during the growing season, depending on their growth stage (Mazahrih et al. 2012). Rahimi et al. (2015) reported that the application of SEBAL for estimating the ETa over agricultural land in the Tajan catchment of Iran resulted in an RMSE of 1.49 mm day^{-1}. However, the daily estimated ETa for both cropland and grassland in the Midwestern United States using SEBAL contributed to RMSE ranging between 1.74 and 2.46 mm day^{-1}(Singh and Senay 2016).

The seasonal validation accuracy assessment between the FAO P-M method and SEBAL model for the different LULC types is shown in Table 3. The RE indicates that the produced daily ETa by the SEBAL model and FAO P-M method is relatively low for the aquatic vegetation and date palm during the summer (Apr–Sep) and winter (Oct–Mar) seasons. However, the RE of the cropland was high in the summer compared to the winter season. Also, the open water showed high RE during both summer and winter seasons. Most of the croplands are cultivated with rice in the summer season, and hence the rice show high ETa during this period. The comparatively high RE of the open water during summer and winter seasons might be attributed to the procedure used for computing the ET_0 between the SEBAL model and the FAO P-M method. The SEBAL model incorporates minimum inputs of routine weather data for the ET_0 calculation, while the FAO P-M method applied more detailed climate data for this purpose.

Table 3 Seasonal validation accuracy of the mean daily ETa for the different LULC types calculated by FAO P-M method and SEBAL model

Season	FAO P-M (mm day^{-1})	SEBAL (mm day^{-1})	Relative error (%)
Water			
Summer	6.37	7.46	14.61
Winter	2.82	3.90	27.70
Aquatic vegetation			
Summer	6.37	6.93	8.10
Winter	2.82	3.32	15.10
Date palm			
Summer	6.37	5.77	10.40
Winter	2.82	2.55	10.59
Cropland			
Summer	6.37	4.91	29.74
Winter	2.82	2.63	7.22

Conclusions

This study demonstrates the power of remote sensing data and biophysical modelling for quantifying the ETa process over an oasis in the arid ecosystem of Saudi Arabia. The estimated mean annual ETa was 2000 mm year^{-1} for open water and varied between 800 and 1400 mm year^{-1} for date palm. However, it was 1600 mm year^{-1} for the aquatic vegetation, while an average of 800 mm year^{-1} was observed in croplands. The validation measure showed a significant agreement level between the SEBAL model and the FAO P-M method with RMSE of 0.62, 0.84, 0.98 and 1.38 mm day^{-1} for aquatic vegetation, date palm, open water and cropland, respectively. However, the seasonal validation accuracy indicated that the predicted ETa by SEBAL model and the measured ETa by FAO P-M resulted in a RE ranged between 7.22 and 29.74% for the different LULC types. The obtained ETa information will help Saudi Arabia formulate strategies to reduce the gap between the water supply and demand in the irrigated areas. Furthermore, the ETa patterns mapped over the diverse LULC systems can be used as a baseline framework for sustainable water resources management and agrometeorological services in the different regions of Saudi Arabia. However, conducting long-term ETa studies using remote sensing data coupled with the implementation of different models and field tools may improve the assessment of the ETa dynamic process in arid regions.

Funding This study is funded by the Deanship of Scientific Research at King Faisal University, under the annual research project (Grant No. 186002).

Declarations

Conflict of interest The authors declare that they have no competing interests.

References

Abdelmoneim H, Soliman MR, Moghazy HM (2020) Evaluation of TRMM 3B42V7 and CHIRPS satellite precipitation products as an input for hydrological model over Eastern Nile Basin. Earth Syst Environ 4:685–698. https://doi.org/10.1007/s41748-020-00185-3

Abungba JA, Khare D, Pingale SM, Adjei KA, Gyamfi C, Odai SN (2020) Assessment of hydro-climatic trends and variability over the Black Volta Basin in Ghana. Earth Syst Environ 4:739–755. https://doi.org/10.1007/s41748-020-00171-9

Al-Dakheel Y (2011) Assessing NDVI spatial pattern as related to irrigation and soil salinity management in Al-Hassa Oasis, Saudi Arabia. J Indian Soc. Remote Sens. 39(2):171–180. https://doi.org/10.1007/s12524-010-0057-z

Alemayehu T, van Griensve A, Senay GB, Bauwens W (2017) Evapotranspiration mapping in a heterogeneous landscape using remote sensing and global weather datasets: application to the Mara Basin, East Africa. Remote Sens. 9:390. https://doi.org/10.3390/rs9040390

Allbed A, Kumar AL, Aldakheel YY (2014) Assessing soil salinity using soil salinity and vegetation indices derived from IKONOS high-spatial resolution imageries: applications in a date palm dominated region. Geoderma 230–231:1–8. https://doi.org/10.1016/j.geoderma.2014.03.025

Allbed A, Kumar AL, Sinha P (2018) Soil salinity and vegetation cover change detection from multi-temporal remotely sensed imagery in Al Hassa Oasis in Saudi Arabia. Geocarto Int. 33(8):830–846. https://doi.org/10.1080/10106049.2017.1303090

Allen RG, Pereira LA, Raes D, Smith M (1998) Crop evapotranspiration. FAO Irrigation and Drainage Paper 56, Rome, ISBN: 92-5-104219-5.

Allen RG, Trezza R, Tasumi M (2006) Analytical integrated functions for daily solar radiation on slopes. Agric for Meteorol. 139:55–73

Allen RG, Tasumi M, Trezza R (2007)Satellite-based energy balance for mapping evapotranspiration with internalized calibration (METRIC)– model. American Society of Civil Engineers. J. Irrig. Drain. E.-ASCE 133380–394.

Allen RG, Pereira SL, Howell TA, Jensen ME (2011) Evapotranspiration information reporting: I. Factors governing measurement accuracy. Agr. Water Manag. 98:899–920. https://doi.org/10.1016/j.agwat.2010.12.015

Allen RG, Trezza R, Tasumi M, Kjaersgaard J (2012) Metric: mapping evapotranspiration at high resolution using internalized calibration. Applications Manual for Landsat Satellite Imagery, Version 2.0.8, March 2012. University of Idaho, Kimberly, Idaho.

Allen RG, Burnett B, Kramber W, Huntington J, Kjaersgaard J, Kilic A, Kelly C, Trezza R (2013) Automated calibration of the metric-landsat evaporation process. J Am Water Resour Assoc. 49(3): 563–576. https://doi.org/10.1111/jawr.12056

Almazroui M, Saeed S, Saeed F, Islam MN, Ismail M (2020) Projections of precipitation and temperature over the South Asian countries in CMIP6. Earth Syst Environ 4:297–320. https://doi.org/10.1007/s41748-020-00157-7

Al-Taher AA (1992) Estimation of potential evapotranspiration in Al-Hassa oasis. Saudi Arabia. Geo. Journal 26(3):371–379

Anderson MC, Allen RG, Morse A, Kustas WP (2012) Use of Landsat thermal imagery in monitoring evapotranspiration and managing water resources. Remote Sens Environ. 122:50–65. https://doi.org/10.1016/j.rse.2011.08.025

Baskauf SJ (2016) Introduction to biological sciences lab (BSCI 1510L) Excel reference and statistics manual. Vanderbilt University, Nashville, TN, USA. http://researchguides.library.vanderbilt.edu/bsci1510L.

Bastiaanssen WGM (2000)SEBAL-based sensible and latent heat fluxes in the irrigated Gediz Basin, Turkey. J. Hydrol. 229:87–100

Bastiaanssen WGM, Menenti M, Feddes RA, Holtslag AAM (1998) Remote sensing surface energy balance algorithm for land (SEBAL): 1. Formulation. J. Hydrol 212-213(1-4)):198–212. https://doi.org/10.1016/S0022-1694(98)00253-4

Bastiaanssen WGM, Molden DJ, Makin IW (2000) Remote sensing for irrigated agriculture: examples from research and possible applications. Agr. Water Manag. 46:137–155. https://doi.org/10.1016/S0378-3774(00)00080-9

Bastiaanssen WGM, Noordman EJM, Pelgrum H, Davids G, Allen RG (2005) SEBAL for spatially distributed ET under actual management and growing conditions. ASCE J. Irrig. Drain. Eng. 131(1): 85–93. https://doi.org/10.1061/(ASCE)0733-9437(2005)131:1(85)

Bellvert J, Adeline K, Baram S, Pierce L, Sanden BL, Smart DR (2018) Monitoring crop evapotranspiration and crop coefficients over an almond and pistachio orchard throughout remote sensing. Remote Sens. 10:2001. https://doi.org/10.3390/rs10122001

Carr MKV (2013) The water relations and irrigation requirements of the date palm (Phoenix dactylifera L.): a review. Expl Agric. 49(1):91–113. https://doi.org/10.1017/S0014479712000993

Chowdhury S, Al-Zahrani M (2015) Characterizing water resources and trends of sector wise water consumptions in Saudi Arabia. JKSUES 27:68–82. https://doi.org/10.1016/j.jksues.2013.02.002

Congalton RG, Green K (2009) Assessing the accuracy of remotely sensed data, principles and practices, 2nd edn. CRC Press, Taylor & Francis Group, Boca Raton

Elhag M, Bahrawi JA (2017) Realization of daily evapotranspiration in arid ecosystems based on remote sensing techniques. Geosci. Instrum. Method. Data Syst. 6:141–147. https://doi.org/10.5194/gi-6-141-2017

ElNesr M, Alazba A, Abu-Zreig M (2010)Spatio-temporal variability of evapotranspiration over the Kingdom of Saudi Arabia. Appl. Eng. Agric. 26(5):833–842

Elnmer A, Khadrc M, Kanaea S, Tawfikb A (2019) Mapping daily and seasonally evapotranspiration using remote sensing techniques over the Nile delta. Agr Water Manag. 213:682–692. https://doi.org/10.1016/j.agwat.2018.11.009

Ghaderi A, Dasineh M, Shokri M, Abraham J (2020) Estimation of actual evapotranspiration using the remote sensing method and SEBAL algorithm: a case study in Ein Khosh Plain, Iran. Hydrology 7:36. https://doi.org/10.3390/hydrology7020036

Gupta N, Banerjee A, Gupta SK (2021)Spatio-temporal trend analysis of climatic variables over Jharkhand, India. Earth Syst Environ 5:71–86. https://doi.org/10.1007/s41748-021-00204-x

Haj-Amor HA, Toth T, Ibrahim MK, Bouri S (2017) Effects of excessive irrigation of date palm on soil salinization, shallow groundwater properties, and water use in a Saharan oasis. Environ. Earth Sci. 76:590. https://doi.org/10.1007/s12665-017-6935-8

Kong J, Hu Y, Yang L, Shan Z, Wang Y (2019) Estimation of evapotranspiration for the blown-sand region in the Ordos basin based on the SEBAL model. Int. J. Remote Sens. 40(5-6):1945–1965. https://doi.org/10.1080/01431161.2018.1508919

Li B, Biswas A, Wang Y, Li Z (2021) Identifying the dominant effects of climate and land use change on soil water balance in deep loessial vadose zone. Agric. Water Manag. 245:106637. https://doi.org/10.1016/j.agwat.2020.106637

Madugundu R, Al-Gaadi KA, Tola E, Hassaballa AA, Patil VC (2017) Performance of the METRIC model in estimating evapotranspiration fluxes over an irrigated field in Saudi Arabia using Landsat-8 images. Hydrol. Earth Syst. Sci. 21:6135–6151. https://doi.org/10.5194/hess-21-6135-2017

Mahmoud SH, Alazba AAA (2016) Coupled remote sensing and the surface energy balance based algorithms to estimate actual evapotranspiration over the western and southern regions of Saudi Arabia. J. Asian Earth Sci. 124:269–283. https://doi.org/10.1016/j.jseaes.2016.05.012

Malbéteau Y, Merlin O, Gascoin S, Gastellu JP, Mattar C (2017) Correcting land surface temperature data for elevation and illumination effects in mountainous areas: a case study using ASTER data over a steep-sided valley in Morocco. Remote Sens. Environ 189: 25–39. https://doi.org/10.1016/j.rse.2016.11.010

Mallick J, Al-Wadi H, Rahman A, Ahmed M (2014) Landscape dynamic characteristics using satellite data for a mountainous watershed of Abha, Kingdom of Saudi Arabia. (2014). Environ Earth Sci 72: 4973–4984. https://doi.org/10.1007/s12665-014-3408-1

Mazahrih NTH, Al-Zubi Y, Ghnaim H, Lababdeh L, Ghananeem M, Abu-Ahmadeh H (2012) Determination of actual crop evapotranspiration and crop coefficient of date palm trees (Phoenix dactylifera) in the Jordan Valley. Am-Euras. J. Agric. & Environ. Sci. 12(4): 434–443

Mohajane M, Essahlaoui A, Fatiha O, El Hafyani M, El Hmaidi A, El Ouali A, Randazzo G, Teodoro AC (2019) Land use/land cover (LULC) using Landsat data series (MSS, TM, ETM+ and OLI) in Azrou Forest, in the Central Middle Atlas of Morocco. Environments 5:131. https://doi.org/10.3390/environments5120131

Mundia CN, Aniya M (2006) Dynamics of land use/cover changes and degradation of Nairobi city, Kenya. Land Degrad. Dev. 17:97–108. https://doi.org/10.1002/ldr.702

Mutiga JK, Su Z, Woldai T (2010) Using satellite remote sensing to assess evapotranspiration: case study of the upper Ewaso Ng'iro North Basin, Kenya. Int. J. Appl. Earth Obs. 12S:S100–S108. https://doi.org/10.1016/j.jag.2009.09.012

Ochege FU, Luo G, Obeta MC, Owusu G, Duulatov E, Cao L, Nsengiyumva JB (2019) Mapping evapotranspiration variability over a complex oasis-desert ecosystem based on automated calibration of Landsat 7 ETM+ data in SEBAL. GISci. Remote Sens. 56(8):1305–1332. https://doi.org/10.1080/15481603.2019.1643531

Oon A, Shafri HZM, Lechner AM, Azhar B (2019) Discriminating between large-scale oil palm plantations and smallholdings on tropical peatlands using vegetation indices and supervised classification of LANDSAT-8. Int. J. Remote Sens. 40(19):7312–7328. https://doi.org/10.1080/01431161.2019.1579944

Qin M, Hao L, Sun L, Liu Y, Sun G (2018) Climatic controls on watershed reference evapotranspiration varied during 1961–2012 in Southern China. J. AM Water Resour 55:189–208. https://doi.org/10.1111/1752-1688.12714

Rahimi S, Sefidkouhi MAG, Raeini-Sarjaz M, Valipour M (2015) Estimation of actual evapotranspiration by using MODIS images (a case study: Tajan catchment). Arch. of Agron. 61(5):695–709. https://doi.org/10.1080/03650340.2014.944904

Rahman MT, Aldosary AS, Mortoja MG (2017) Modeling future land cover changes and their effects on the land surface temperatures in the Saudi Arabian Eastern Coastal City of Dammam. Land 6:36. https://doi.org/10.3390/land6020036

Sentelhas PC, Gillespie TJ, Santos EA (2010) Evaluation of FAO Penman-Monteith and alternative methods for estimating reference evapotranspiration with missing data in Southern Ontario, Canada. Agric. Water Manag. 97:635–644. https://doi.org/10.1016/j.agwat.2009.12.001

Singh RK, Senay G (2016) Comparison of four different energy balance models for estimating evapotranspiration in the Midwestern United States. Water 8:9. https://doi.org/10.3390/w8010009

Sun H, Yang Y, Wu R, Gui D, Xue J, Liu Y, Yan D (2019) Improving estimation of cropland evapotranspiration by the Bayesian model averaging method with surface energy balance models. Atmosphere 10:188. https://doi.org/10.3390/atmos10040188

USGS (2019) Department of the Interior United State Geological Survey (USGS). Landsat 8 (L8) data users handbook. LSDS-1574 Version 5.0. https://www.usgs.gov/media/files/landsat-8-data-users-handbook.

Yang L, Fenga Q, Adamowski JF, Alizadeh MR, Yin Z, Wen X, Zhua M (2021) The role of climate change and vegetation greening on the variation of terrestrial evapotranspiration in northwest China's Qilian Mountains. Sci. Total Environ. 759:143532. https://doi.org/10.1016/j.scitotenv.2020.143532